

◇ MONOGRAPH EXCERPT ◇

MATTER ANTIMATTER FLUCTUATIONS

SEARCH, DISCOVERY AND ANALYSIS OF B_s FLAVOR OSCILLATIONS

NUNO LEONARDO

Complete work published as:

Analysis of B_s oscillations at CDF, MIT Thesis (2006)

Matter antimatter fluctuations, Monograph, LAP Lambert (2011)

Author © Nuno Teotónio Leonardo

Chapter 3

Experimental apparatus

The Tevatron, at the time the research analysis is performed, is the world's highest energy accelerator. It is lodged in an underground ring with radius of about 1 km located at the Fermi National Accelerator Laboratory (Fermilab), Illinois, USA. Protons and antiprotons ($p\bar{p}$) are brought into collision with a center of mass energy of approximately 1.96 TeV. The collisions take place at two points separated by about 120° along the ring. The CDF detector, which collects the data analyzed in this dissertation, surrounds one such collision point. The other collision point lays at the center of the $D\bar{O}$ detector. Both the accelerator and the collider detectors underwent major upgrades between 1997 and 2001, mainly aimed at achieving, and to cope with, higher luminosities. The upgraded machine accelerates 36 bunches of protons and antiprotons, resulting in a time between bunch crossings of 396 ns. The period in which the current data is taken is referred to as the Run II of Tevatron and the detector is referred as CDF II. In the following sections we first outline the Fermilab accelerator complex, and describe the components of the CDF II detector, data taking structure and trigger systems used to collect and measure the properties of the particles produced in the $p\bar{p}$ collisions.

3.1 The Tevatron collider

In order to create the world's most powerful particle beams, Fermilab uses a series of accelerators. The diagram in Figure 3.1 shows the paths taken by protons and antiprotons from initial acceleration to collision in the Tevatron.

Proton source

The process leading to the production of $p\bar{p}$ colliding beams is initiated with a Cockcroft-Walton [34] pre-accelerator. Negatively charged ions H^- are created from the ionization of

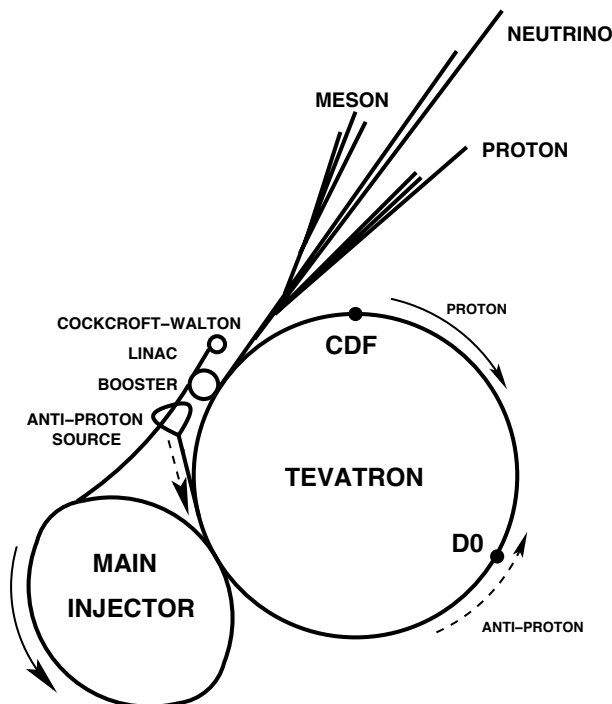


Figure 3.1: Layout of the Fermilab accelerator complex.

hydrogen gas and accelerated to a kinetic energy of 750 keV. The H^- ions are delivered to a 150 m long linear accelerator (Linac) [35]. The Linac uses a radio-frequency (RF) field, running at about 800 MHz, to further accelerate the H^- ions to an energy of 400 MeV. Before entering the next stage, a carbon foil removes the electrons from the H^- ions, leaving only the protons. The 400 MeV protons are then injected into the Booster, a 74.5 m diameter circular synchrotron [35]. The intensity of the proton beam is increased by injecting new protons into the same orbit as the circulating ones. The protons travel around the Booster about 200,000 times to a final energy of 8 GeV. Protons emerge from the Booster in 84 bunches, with about 6×10^{10} protons each, spaced by about 19 ns.

Main Injector

Protons are extracted from the Booster into the Main Injector [36], a synchrotron of about 3 km in circumference which operates at 53 MHz. The Main Injector accelerates both protons and antiprotons from 8 GeV to 150 GeV. The bunches are also coalesced into 36 bunches per beam, before being finally injected into the Tevatron, where they undergo the final acceleration stage.

The Main Injector accomplishes further duties, which include the acceleration of protons to 120 GeV to be delivered to fixed target areas, the NuMI beamline for neutrino production,

and the antiproton production target.

Antiproton production

One major advantage of a $p\bar{p}$ collider is that the proton and antiproton beams can circulate in opposite directions sharing the same magnet and vacuum systems. One major disadvantage of using \bar{p} beams, nevertheless, is the associated cost of production. In the absence of technical problems with the accelerator such as system-to-system transfer inefficiencies, antiproton supply constitutes the most limiting factor for attaining higher luminosities.

The antiprotons are produced using a proton pulse of 120 GeV from the Main Injector, which is directed onto a nickel target. In the collisions, about 20 antiprotons are produced per one million incident protons, with a mean kinetic energy of 8 GeV. The produced antiprotons are collected and focused by a lithium lens and separated from the other by-products of the proton-nickel scattering using a bending magnet.

Exiting the collecting lens, the antiprotons have a large spread of momentum in longitudinal and transverse directions. Before being accelerated and further prepared for collisions, the particles must be confined to a smaller phase space volume. As this condition thermodynamically corresponds to a lower temperature, the process is referred to as beam *cooling*. Antiprotons are initially cooled in the Debuncher collected and further cooled using stochastic cooling [37] in the Accumulator. Stochastic cooling is a feedback-based method, where the particles' motion is sampled with pickup sensors placed around the beam, and their trajectories corrected with kicker electrodes and magnets. Such distinctive efforts are needed for obtaining cold antiproton beams without significant antiproton loss; protons, on the other hand are more readily available, and consequently cold beams may in this case be more simply produced by removing particles found outside the desired phase space volume. The *stacking* of antiprotons in the Accumulator, depending on the desired beam intensity, may take up to a day. The antiprotons have at this stage a characteristic energy of 8 GeV, with reduced beam size and momentum spread.

The stacked antiprotons, in a bunched beam configuration identical to that of the protons, are delivered back into the Main Injector. There they are accelerated to 150 GeV to be transferred next to the Tevatron for final acceleration and collision. Not all antiprotons are used during a *store* (time period of stable circulation that the colliding $p\bar{p}$ beams are retained in the Tevatron). The Recycler ring makes the recovery of these antiprotons (which amount to about 75% of the original injection quantity) possible for use in a later store, thus significantly reducing the stacking time. The Recycler is installed in the Main Injector enclosure, and functions as an antiproton storage ring. By storing antiprotons in the Recycler high antiproton intensities can be achieved as the stacking rate in the Accumulator is reduced

at high antiproton intensities.

Tevatron

The final stage of Fermilab's accelerator chain is the Tevatron. It receives 150 GeV protons and antiprotons from the Main Injector and accelerates them to 980 GeV. The protons and antiprotons circle the Tevatron in opposite directions. The beams are brought to collision at the center of the two detectors, CDF II and DØ.

The antiprotons are loaded after the protons have been injected. Before antiproton injection, a set of electrostatic separators are used to create a pair of non-intersecting closed helical orbits with the protons circulating on one strand of the helix and the antiprotons on the other. This provides transverse separation of the proton and antiproton bunches as they pass each other at crossing points other than CDF and DØ.

Once loading is complete beams are accelerated to the maximum energy and collisions are initiated. Both protons and antiprotons circulate in three trains of 12 bunches, separated by about 2.6 μs , with bunches in each group spaced by 396 ns. After acceleration is complete, the beams are further focused in the CDF and the DØ interaction regions, the transverse size being reduced from about 1 mm to about 25 μm . This results in an increase of the chance of a proton and antiproton colliding.

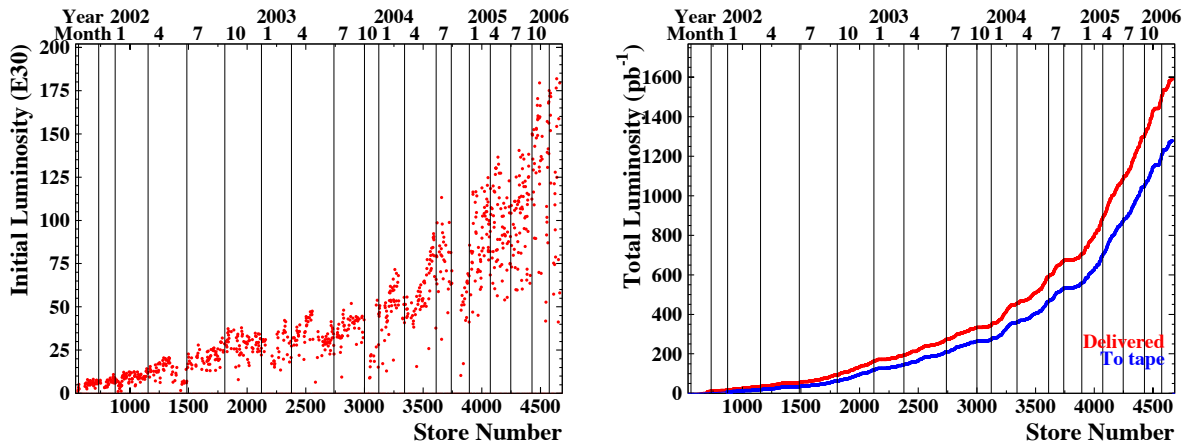
The *instantaneous luminosity*, to which the rate of collisions is proportional, in the absence of a crossing angle or offset in beams position, is approximately given by

$$L = \frac{f N_B N_p N_{\bar{p}}}{2\pi(\delta_p^2 + \delta_{\bar{p}}^2)} F \left(\frac{\delta_l}{\beta^*} \right), \quad (3.1)$$

where f is the bunch revolution frequency, N_B is the number of bunches, $N_{p(\bar{p})}$ is the number of protons (antiprotons) per bunch, and $\delta_{p(\bar{p})}$ is the protons (antiprotons) *rms* beam size at the interaction point. F is a form factor which corrects for the bunch shape and depends on the ratio of the bunch length δ_l to the beta function β^* at the interaction point (the beta function is a measure of the beam width, and it is proportional to the beam's x and y extent in phase space). The Run II design parameters are summarized Table 3.1. The *integrated luminosity*, defined as $\mathcal{L} = \int L dt$, is more relevant to physics analyses. The probability of occurrence for interactions is directly proportional to the cross section of the process σ [cm^2] and to \mathcal{L} [cm^{-2}]. For cross sections observed at high energy collisions the preferred basic unit is the *barn* ($b = 10^{-24}\text{cm}^2$). The integrated luminosity delivered by the accelerator along with that recorded by CDF are illustrated in Figure 3.2.

number of bunches (N_B)	36
bunch rms [m]	0.37
bunch spacing [ns]	396
protons/bunch (N_p)	2.7×10^{11}
antiprotons/bunch ($N_{\bar{p}}$)	3.0×10^{10}
total antiprotons	1.1×10^{12}
β^* [cm]	35
interactions/crossing	2.3
peak luminosity [$\text{cm}^{-2}\text{s}^{-1}$]	1.2×10^{32}

Table 3.1: Tevatron Run II parameters.

Figure 3.2: Initial luminosity [$\text{cm}^{-2}\text{s}^{-1}$] per Tevatron store (left), and integrated luminosity [pb^{-1}] delivered and recorded (right).

3.2 The CDF II detector

The Collider Detector at Fermilab (CDF) is a general-purpose, azimuthally and forward-backward symmetric apparatus designed to study $p\bar{p}$ collisions at the Tevatron. Its design, accordingly, rather than being tailored toward a specific class of physics measurement, is optimized toward extracting different properties of all particle species emanating from the $p\bar{p}$ collisions. A diagram of the CDF II detector is shown in Figure 3.3.

The innermost detector system is the integrated tracking and vertexing system. It consists of a Silicon microstrip detector and a multi-wire drift chamber, which have a cylindrical geometry concentric with the beam. It is designed to detect charged particles, measure their trajectories and momenta. Reconstructed particle trajectories are referred to as *tracks*. Multiple track reconstruction allows the identification of vertices, where either the $p\bar{p}$ interaction occurred (primary vertex) or the decay of a long-lived particle took place (secondary or displaced vertex).

The tracking system is surrounded by the time-of-flight (TOF) system, designed to provide particle identification for low-momentum charged particles. Both the tracking and time-of-flight systems are placed inside a superconducting coil, which generates a 1.4 Tesla solenoidal magnetic field parallel to the beam axis. The coil is surrounded by electromagnetic and hadronic calorimeters, which measure the energy of particles that shower when interacting with matter. The calorimetry systems are surrounded by the muon detector system. Muons interact with matter primarily through ionization, and act as minimally ionizing particles depositing only small amounts of ionization energy. Therefore, they are able to penetrate through the tracking, TOF, solenoid and calorimeter systems, with minimal interaction with the detector material. The muon chambers, therefore, are located radially outside the calorimeters.

All of the detector parts mentioned above provide information which is used in the analyses presented in this monograph, and will be described in the following sections. A more complete and detailed description of the CDF II detector can be found in the Technical Design Reports [38].

Unlike in e^+e^- collisions, in $p\bar{p}$ collisions not all of the center of mass energy of the $p\bar{p}$ system is absorbed by the participants in the fundamental interaction. It is the partons inside the proton and antiproton (valence or sea quarks, or gluons) that are involved in the fundamental interactions, and these carry only a fraction of the proton and antiproton momenta. Furthermore, as a result of a possible imbalance in the momenta of the two interacting partons, the observed physics interactions often have large boosts along the beam direction (the “longitudinal” direction). That is not the case on the plane perpendicular

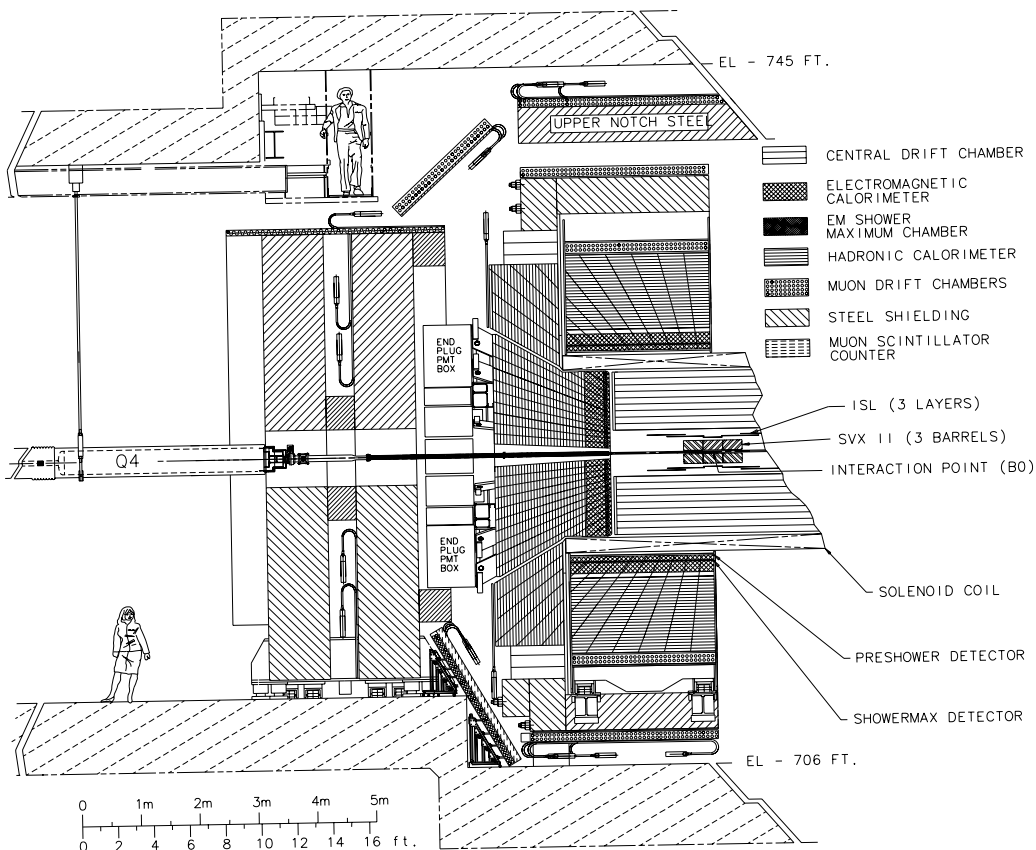
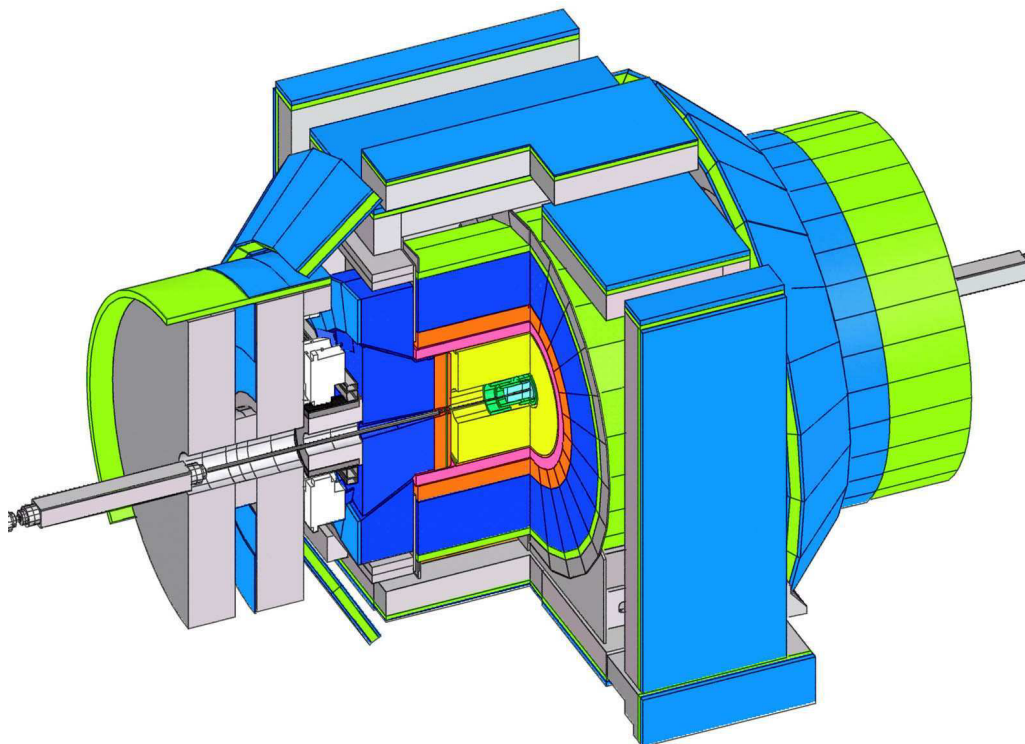


Figure 3.3: The CDF II detector with a quadrant cut (top) and elevation view (bottom) exposing the different sub-detectors.

(“transverse”) to the beam, given the negligible transverse motion of the colliding particles. It follows, for instance, that the vectorial sum of all particles’s transverse momenta in a collision vanishes.

The geometrical center of the detector, roughly coincident with the beam crossing region, serves as the origin for the CDF coordinate systems. In the Cartesian system, the x axis is in the (horizontal) plane of the accelerator, pointing radially outward, and the y axis points upwards. The beams travel through the detector approximately parallel to the z axis, with protons moving in the positive z direction. The detector’s barrel-like shape makes it convenient to introduce cylindrical (r, ϕ, z) or polar (ρ, ϕ, θ) coordinates. The r and ρ coordinates indicate the associated radial distances from the origin, and ϕ is the azimuthal angle. The r - ϕ (or x - y) plane is referred as the *transverse plane*, as it is perpendicular to the beam line. The polar angle θ is defined relative to the z axis. It is convenient to introduce yet another variable, as an alternative to the polar angle; namely, the pseudorapidity η is defined as

$$\eta \equiv -\ln \tan \left(\frac{\theta}{2} \right). \quad (3.2)$$

This quantity coincides with the ultrarelativistic, massless limit of a particle’s rapidity

$$y \equiv \frac{1}{2} \ln \frac{E + p_z}{E - p_z}. \quad (3.3)$$

Differences in y , and in the mentioned limit therefore also in η , are invariant under Lorentz boosts along the z direction. The angular variable η is often used for specifying the geometrical coverage of the detector sub-systems. The variable

$$\Delta R \equiv \sqrt{\Delta\phi^2 + \Delta\eta^2} \quad (3.4)$$

is commonly used for specifying angular distances.

3.2.1 Tracking and vertexing

Charged particles cause ionization as they pass through matter, leaving trails of charge and energy clusters, denoted *hits*, along their paths. Once detected, hits can be used to reconstruct the particles’ trajectories, in the process known as *tracking*. From the intersection of multiple reconstructed tracks, *vertices* may be obtained.

CDF’s innermost tracking device is a silicon microstrip vertex detector, which consists of three concentric systems. A layer of silicon sensors, called Layer 00 (L00) [39], is installed directly onto the beryllium vacuum beam pipe, with the sensors at radii 1.35 and 1.62 cm from the beam. The layer of silicon on the beam pipe is followed by five concentric layers

of silicon sensors, denoted the Silicon Vertex Detector SVX [40], located at radii between 2.45 and 10.6 cm. The Intermediate Silicon Layers, ISL [41], are the outermost silicon sub-detector systems, consisting of one layer at a radius of 22 cm in the central region and two layers at radii 20 and 28 cm in the forward regions. L00 provides $r-\phi$ information, while SVX and ISL provide both $r-\phi$ and z measurements.

Surrounding the silicon detector is the Central Outer Tracker (COT) [42], a 3.1 m-long cylindrical open-cell drift chamber covering radii from 40 to 137 cm. The layout of the systems is shown in Figure 3.4.

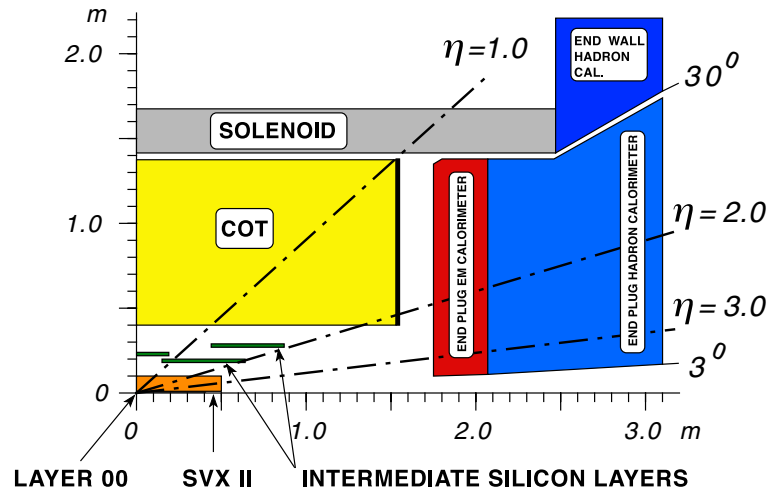


Figure 3.4: The CDF II tracker layout showing the different sub-detector systems.

Silicon vertex detectors

A silicon tracking detector is fundamentally a reverse-biased p-n junction. The passage of a charged particle leaves a trail of electron-hole pairs induced by ionization, which drift in opposite directions in the existing electric field. The reverse-biased voltage increases the gap between the conduction and valence bands across the p-n junction and reduces the current from thermal excitation. By segmenting the p or n side of the junction into finely spaced *strips* and reading out the charge deposition separately on every strip, a well-localized signal is obtained. The typical distance between two strips is about $60 \mu\text{m}$. Charge deposition from a single particle passing through the silicon sensor will usually be detected on a *cluster* of strips rather than just one. The hit position is extracted by weighting the strip positions by the amount of charge collected.

There are two types of microstrip detectors: single and double-sided. In single-sided detectors only one (p) side of the junction is segmented into strips. Double-sided detectors

	layer 0	layer 1	layer 2	layer 3	layer 4
number of ϕ strips	256	384	640	768	869
number of z strips	256	576	640	512	869
stereo angle	90°	90°	+1.2°	90°	-1.2°
ϕ strip pitch [μm]	60	62	60	60	65
z strip pitch [μm]	141	125.5	60	141	65
active width [mm]	15.30	23.75	38.34	46.02	58.18
active length [mm]	72.43	72.43	72.38	72.43	72.43

Table 3.2: Relevant parameters for the layout of the sensors of the SVX layers.

have both sides of the junction segmented into strips. The benefit of double-sided detectors is that while one (p) side has strips parallel to the z direction, providing ϕ position measurements, the other (n) side can have strips at an angle (stereo angle) with respect to the z direction, which will give z position information. The innermost layer, L00, is made of single-sided silicon sensors which only provide $r-\phi$ measurements. The SVX and ISL are made of double-sided silicon sensors. As shown in Table 3.2, the SVX layers have different stereo angles. Two layers have a 1.2° stereo angle and three have a 90° stereo angle. The ISL detector provides small angle (1.2°) stereo information.

The SVX silicon sensors are supported by carbon fiber rails in assemblies called *ladders*. Each ladder hosts four pieces of silicon sensors, whose readout electronics are mounted directly to the surface of the silicon sensor at each end of the ladder. Each of the 5 SVX concentric layers is formed of 12 ladders in ϕ , with a small overlap at the edges for improved coverage. The ladders are further arranged in three, 29 cm long barrels, mounted end-to-end along the z axis. Each barrel contains a total of 60 ladders, mounted between two beryllium bulkheads which provide mechanical support and which also carry the water cooling lines for the readout electronics.

The coverage of the silicon detector sub-systems is shown in Figure 3.5.

Drift chamber

The Central Outer Tracker, COT [42], is a cylindrical multi-wire open-cell drift chamber. with a coverage of $|\eta| < 1$. The system is segmented into 8 concentric *superlayers*, as represented in Figure 3.6. A superlayer is divided into *cells* in ϕ . Each cell contains 12 sense wires and 17 potential (for field shaping) wires along with adjacent ground field (cathode) sheets on either side. The potential wires alternate with the sense wires at a pitch of 0.3556 cm. The distance between the wires and the field sheets is 0.88 cm. Both the sense and the potential

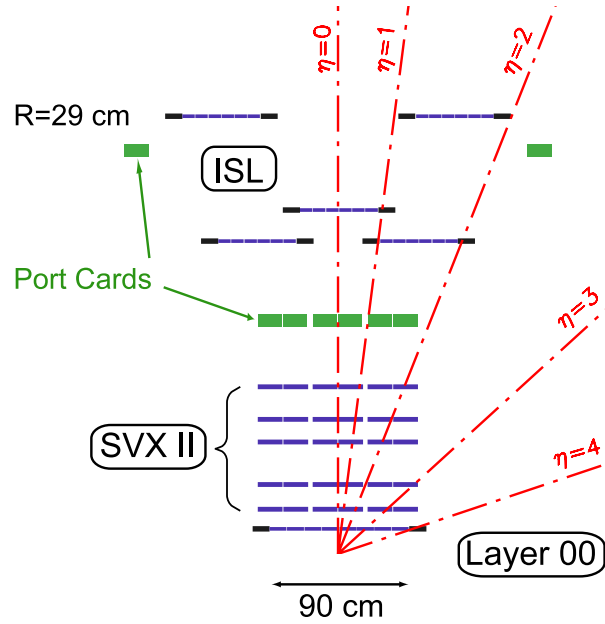


Figure 3.5: Coverage of the different silicon sub-detectors projected into the $r-z$ plane; the r and z axes have different scales.

wires are $40 \mu\text{m}$ diameter gold plated Tungsten. The field sheets are $6.35 \mu\text{m}$ thick Mylar with vapor-deposited gold on both sides, and are shared among adjacent cells. The cells layout is shown in Figure 3.7.

The maximum drift distance is approximately the same for all superlayers. Thus, the number of cells in a given superlayer scales approximately with the radius of the superlayer. The entire COT contains 30,240 sense wires. The wires in superlayers 2, 4, 6 and 8 run along the z direction (“axial”), while the wires in the other superlayers are strung at a small angle (2°) with respect to the z direction (“stereo”).

The COT chamber is filled with an Argon-Ethane gas mixture and Isopropyl alcohol (49.5:49.5:1). The voltages on the sense wires are 2600-3000 volts and 1000-2000 volts on the potential wires; the ground sheets are grounded. Charged particles that pass through the gas mixture leave a trail of ionization electrons. The electric field created by the cathode field sheets and the potential wires cause the electrons to drift toward the sense wires; the drift velocity is $\sim 50\mu/\text{ns}$. Due to the magnetic field in which the COT is immersed, electrons drift at a Lorentz angle of $\sim 35^\circ$. Therefore, the cell is tilted by 35° with respect to the radial direction to compensate for this effect. After the tilt the electrons drift approximately perpendicularly to the wire plane. The maximum electron drift time is less than 200 ns, much shorter than the bunch crossing frequency of 396 ns.

When the ionization electrons drift close to the wires surface the local $\frac{1}{r}$ electric field

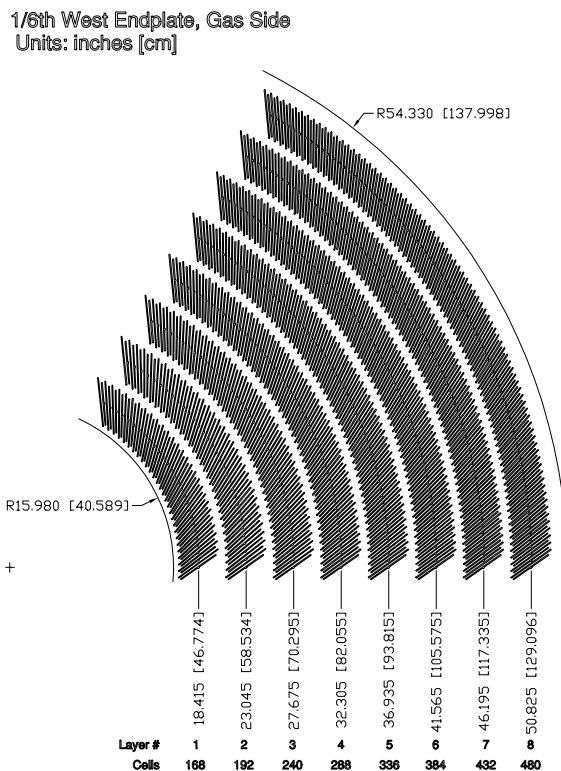


Figure 3.6: Layout of wire planes on a COT endplate.

vigorously accelerates them. This further causes secondary ionization thus initiating a limited avalanche, which produces a signal (hit) on the wire large enough to be read out by the electronics attached to the end of the wire. Signals on the sense wires are processed by the ASDQ (amplifier, shaper, discriminator with charge encoding) chip, which provides input protection, amplification, pulse shaping, baseline restoration, discrimination and charge measurement [43]. The leading edge gives the arrival time information and the pulse width encodes the amount of charge collected by the wire. Upon calibration the digital width is thus used in the measurement of the ionization energy loss along the trail of the particle through the COT, dE/dx , for particle identification. The pulse is sent through ~ 105 cm of micro-coaxial cable, via repeater cards to time to digital converter (TDC) boards in the collision hall. Hit times are later processed by pattern recognition software to form helical tracks. The hit resolution of the COT is about $140 \mu\text{m}$. The transverse momentum (p_T) resolution is $\sigma_{p_T}/p_T \sim 0.15\% \cdot p_T$.

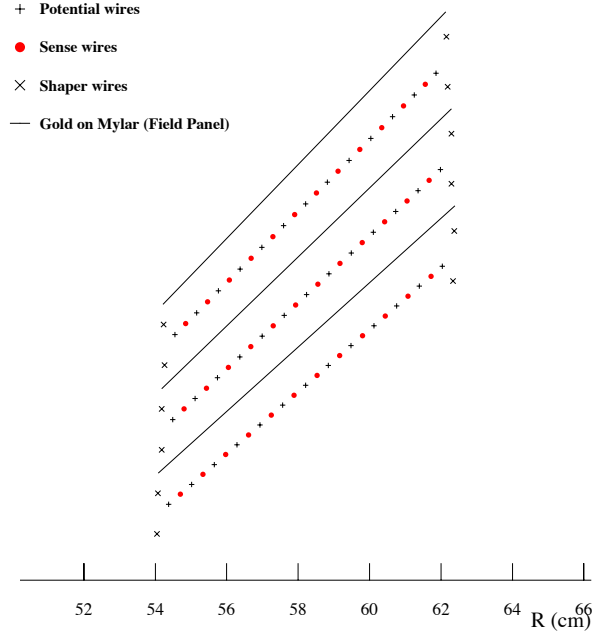


Figure 3.7: Transverse view of three adjacent COT cells.

Track reconstruction

Charged particles moving through a uniform solenoidal magnetic field, such as that which permeates the CDF tracking volume, follow helical trajectories. To uniquely describe such a trajectory in three dimensions five parameters are needed. Three of those parameters are chosen to describe a position and two more are associated to the momentum vector at that position. Specifically, the set of parameters is: C , $\cot \theta$, d_0 , ϕ_0 , z_0 . The latter three correspond to the r , ϕ and z cylindrical coordinates of the point of closest approach of the helix to the z axis, C is the helix curvature and θ is the angle between the z axis and the particle's momentum vector.

The projection of the helix on the transverse r - ϕ plane is a circle. The curvature C is a signed quantity given by $C = \frac{q}{2R}$, where R is the radius of the circle and the signal of the particle's charge q is given by its bending direction in the magnetic field. The transverse momentum p_T can be calculated from the helix curvature and magnetic field (B_{solenoid}) as

$$p_T = \frac{cB_{\text{solenoid}}}{2|C|}. \quad (3.5)$$

The longitudinal momentum p_z component can then be also calculated as $p_z = p_T \cdot \cot \theta$. The direction of the transverse momentum vector \vec{p}_T is implicitly given by ϕ_0 , noting that at any given point of the helix the track momentum is tangent to the helix.

The *impact parameter* d_0 of a track is a signed variable, whose absolute value corresponds to the distance of closest approach of the track to the beamline. It is defined as

$$d_0 = q \cdot \left(\sqrt{x_c^2 + y_c^2} - R \right), \quad (3.6)$$

where (x_c, y_c) is the center of the helix as projected onto the x - y plane.

Pattern recognition

The process of track reconstruction begins using only COT information. The COT electronics report hit time and integrated charge (codified as the leading edge and width of the digital pulse, respectively, from the TDC) for every sense wire. The hit locations are reconstructed from the time difference between when the ionization occurs (the collision time plus the particle's time of flight) and when the signal is picked up by the wire. Corrections from the global time offset of the wires and cables, electronic channel pedestals, charged-based time slewing and non-uniform drift velocities are accounted for.

The first step in pattern recognition is to look for circular paths in the axial superlayers of the COT. Sets of 4 or more hits are searched for in each axial superlayer to form a straight line, or *segment*. Once segments are found, there are two approaches to track finding. One approach is to link together segments for which the measurements of curvature and ϕ_0 are consistent with lying tangent to a common circle. The other approach is to constrain the circular fit to the beamline starting from the outermost superlayer, and then add hits which are consistent with this path. Once a circular path is found in the r - ϕ plane, segments and hits in the stereo superlayers are added depending on their proximity to the circular fit. This results in a three-dimensional track fit. Typically, if one algorithm fails to reconstruct a track, the other algorithm will not.

Once a track is reconstructed in the COT, it is extrapolated into the SVX. A three-dimensional "road" is formed around the extrapolated track, based on the estimated errors on the track parameters. Starting from the outermost layer, and working inward, silicon clusters found inside the road are added to the track. As a cluster is added, a new track fit is performed, which modifies the error matrix for the track parameters and produces a narrower road. In the first pass of this algorithm, r - ϕ clusters are added. In the second pass, clusters with stereo information are added to the track. If there are multiple tracks with differing combinations of SVX hits associated with the same COT track, the track with the largest number of SVX hits is chosen.

The track reconstruction efficiency in the COT is about 95% for tracks which pass through all 8 superlayers ($p_T \geq 400$ MeV/ c), and 98% for tracks with $p_T \geq 10$ GeV/ c . It depends mostly on the number of tracks present, as hits from one track can shadow hits from the

other track. The track reconstruction efficiency for the addition of SVX information is about 93% for tracks with at least 3 SVX $r-\phi$ hits.

Vertexing

A particle's production point cannot be inferred from a reconstructed helix alone. In general its production vertex is found from the intersection with one or more helices associated with particles assumed to have originated from the same space point. The process of finding the spatial coordinates, along with corresponding uncertainties, of the tracks' intersection point is referred to as *vertexing*. Algorithms employed at CDF for this purpose are described in [44].

For decaying particles, we define the displacement L_{xy} as

$$L_{xy} = \vec{d} \cdot \hat{p}_T, \quad (3.7)$$

where \vec{d} is the displacement vector of the decay vertex in the transverse plane, and \hat{p}_T is the unit vector in the direction of \vec{p}_T .

3.2.2 Calorimetry

Surrounding the CDF tracking volume, and outside the solenoid coil, are found the electromagnetic (EM) calorimeters followed by the hadronic (HA) calorimeters. Comparison of the energy deposition in the electromagnetic and the hadronic calorimeters provides separation between electrons and photons (whose energy is mostly absorbed in the electromagnetic calorimeter) and hadrons (which deposit a large fraction of their energy in the hadronic calorimeter).

The calorimeter detectors are segmented in η and ϕ towers that point to the interaction region, in an arrangement referred to as projective tower geometry. The calorimeter system is divided into *central*, *wall* and *plug* regions. They are denoted central electromagnetic (CEM), central hadronic (CHA), wall hadronic (WHA), plug electromagnetic (PEM) and plug hadronic (PHA) sub-systems. The central calorimeters cover the pseudorapidity region of about $|\eta| < 1$. Each tower spans 15° in azimuth and about 0.1 in pseudorapidity. Plug calorimeters extend the pseudorapidity coverage to $|\eta|=3.6$, and use variable segmentation: 7.5° to 15° in ϕ , and 0.1 to 0.6 in $|\eta|$.

The CEM and PEM towers consist of lead sheets interspersed with scintillator as the active detector medium. The light signal is wavelength-shifted and carried by light guides to the photomultiplier tubes (PMTs), which measure the number of scintillation photons produced in the EM shower that is formed during the particles' passage through the detector. Both calorimeters are equipped with shower maximum detectors, CES and PES for central and

	η coverage	thickness	energy resolution [%]
CEM	$ \eta < 1.1$	$19X_0$	$13.5/\sqrt{E \sin \theta} \oplus 2$
PEM	$1.1 < \eta < 3.6$	$21X_0$	$16/\sqrt{E \sin \theta} \oplus 1$
CHA	$ \eta < 1.1$	$4.5\lambda_0$	$75/\sqrt{E \sin \theta} \oplus 3$
WHA	$0.7 < \eta < 1.3$	$4.5\lambda_0$	$75/\sqrt{E \sin \theta} \oplus 3$
PHA	$1.3 < \eta < 3.6$	$7\lambda_0$	$80/\sqrt{E \sin \theta} \oplus 5$

Table 3.3: Pseudorapidity coverage, thickness, and energy resolution (with E in GeV) for the different calorimeter sub-detectors of CDF II; λ_0 signifies interaction length and X_0 radiation length.

plug regions respectively. These are proportional chambers of wires and strips, embedded at the depth of about 6 radiation lengths (X_0), which measure the coordinates of showers produced by electrons and photons with 1-3 mm accuracy. Shower maximum detectors are used for identification of electrons and photons by matching the position of electromagnetic showers with incident tracks. They also provide measurements of the transverse shower profile which are used to separate photons from neutral pions, and the pulse height helps to identify electromagnetic showers. Another set of multi-wire proportional chambers is located between the solenoid coil and the CEM at a radius of about 168 cm. These constitute the preshower detector (CPR), which samples the electromagnetic showers that begin in the solenoid material ($1.08 X_0$), providing enhanced soft electron identification and separation from lesser ionizing particles such as muons and pions.

The hadronic calorimeters are located immediately behind the electromagnetic calorimeters, with matching segmentation. The CHA and WHA towers are formed of alternating layers of iron and scintillator. The pseudorapidity coverage, thickness and resolutions for the different electromagnetic and hadronic calorimeters are given in Table 3.3. A detailed description can be found in [38].

3.2.3 Muon chambers

The radially outermost component of CDF II is the muon system, which comprises sets of drift chambers and scintillators. While electrons and hadrons deposit most of their energy in the calorimeter material, muons which are minimum ionizing penetrate much more material than any other charged particles, and given enough momentum reach the muon chambers. There they leave a track segment, called a muon *stub*. If a stub matches a track measured in the COT then the two are combined to form a muon candidate.

The CDF II detector contains four muon systems: the central muon (CMU), the central muon upgrade (CMP), the central muon extension (CMX), and the intermediate muon (IMU) detectors [45]. The coverage of each sub-system is represented in Figure 3.8.

The CMU detector is located around the outside of the central hadronic calorimeter at a radial distance of 347 cm. It is segmented in ϕ into 24 wedges, with a gap of 2.4° between wedges which limit the coverage in ϕ to about 84%. The CMU is also divided into East (positive z) and West (negative z) halves with about a 18.4 cm gap at $\eta = 0$ between the two. Each wedge is further segmented azimuthally into three 4.2° modules; there is a total of 144 modules. A module consists of 4 layers of 4 rectangular drift cells. A cell has at its middle a 226 cm long, $50 \mu\text{m}$ stainless steel sense wire, parallel to the z axis, and is filled with an identical (Argon-Ethane-alcohol) gas mixture as the COT.

The CMP consists of drift chambers located behind a 60 cm iron shield. The CMP chambers are comprised of rectangular ($2.5 \text{ cm} \times 15 \text{ cm} \times 640 \text{ cm}$), single-wire drift tubes configured in four layers with alternate half-cell staggering. In combination with the CMU, the CMP improves further the purity of muon identification. Muon candidates with stubs in both CMU and CMP are referred to as CMUP muons.

The CMX detector provides an extension to the central muon systems to cover $0.6 < |\eta| < 1.0$. It is a conical arrangement of drift tubes similar to those of CMP cells and a sandwich of scintillators. It has a 30° gap (top, East) which is filled with the instrumentation for the solenoid cryogenic system. The CMX is azimuthally segmented in 15° wedges, each made up of 8 layers of drift tubes. The tubes are 180 cm long, have a rectangular cross-section, and are staggered.

The IMU consists of a barrel of drift chambers and scintillator counters mounted on the outer radius of two (non-energized) steel toroids with additional counters between the toroids, in a pseudorapidity region of $1.0 < |\eta| < 1.5$. The chambers and counters are similar to those in the CMP. Each chamber covers 12.5° in azimuth, and is about 363 cm long.

Shielding serves the desired duty of preventing hadrons from reaching the muon chambers. The effective hadronic shielding provided mostly by calorimeters, solenoid coil, and additional steel absorbers in the path to each muon sub-system is quantified in Table 3.4 in terms of pion interaction lengths. While an increasing amount of absorber improves muon purity, it also causes muons themselves to lose energy. As a result, muons below certain momentum thresholds do not reach the muon detectors; the rangeout thresholds for the individual systems are summarized in Table 3.4. Another issue is Coulomb scattering, the effect of which becomes amplified with the introduction of additional material. Multiple Coulomb scattering randomly deflects a particle's path through the material, inducing deviations of the detected trajectory in the muon system from that expected by extrapolation from the

tracking volume.

It remains possible, however, that a small fraction of hadrons that interact late in the calorimeters will produce secondary particles that still reach the muon chambers; these are referred to as *punch-throughs*. Additional background may be due to real muons from decays of pions and kaons, referred to as *decays-in-flight*, or simply to fake stubs produced by electronic noise.

Track-stub matching

Muon candidates are reconstructed by matching the stub position in the muon detector to a track measured in the COT and extrapolated to the muon chambers. Using the timing information from the drift cells of the muon systems, hit positions are found. A muon stub is obtained by fitting sets of hits using a least-square method to a segment line. A stub must have at least 3 hits associated to it. Stubs need then to be matched to COT tracks. For stubs reconstructed in the CMU, CMP, CMX and IMU, the set of tracks with transverse momentum above 1.4 GeV/c, 2.2 GeV/c, 1.5 GeV/c and 2.5 GeV/c, respectively, are considered. The tracks are extrapolated using a simplified geometry model of the muon candidate's motion in the non-uniform magnetic field in the calorimeter.

The matching procedure compares the position of the stub in a given muon chamber with the extrapolated position of the track. Differences in position and direction, along with stub χ^2 and track covariance matrix are used. The evaluated match distance in the $r-\phi$ plane between the projected track and the stub, denoted ΔX , is required to be smaller than 30 cm, 60 cm, 50 cm and 90 cm, respectively, for CMU, CMP, CMX and IMU muons. The mentioned matching and minimum momentum requirements are chosen in order to maximize the muon reconstruction efficiency while maintaining high muon purity.

Additional matching variables are further defined and evaluated, which serve as discriminating variables for muon identification. These include, for all muon sub-systems, the opening angle $\Delta\Phi$ between the stub and the direction of the track extrapolation, projected on to the $r-\phi$ plane. The distance in the $r-z$ plane, denoted ΔZ , is evaluated for all muon types except CMP (the CMP chambers measure the location of the stub in the $r-\phi$ plane only). Additional information such as the number of hits used to reconstruct the stub, and the χ^2 fit of the stub are also provided.

3.2.4 Time of flight

Outside the tracking system, but still inside the superconducting magnetic coil, CDF II has a time-of-flight (TOF) [46] system. It is designed to distinguish low momentum pions, kaons

	η coverage	pion interaction length	minimum muon p_T
CMU	$ \eta < 0.6$	5.5	1.4 GeV/c
CMP	$ \eta < 0.6$	7.8	2.2 GeV/c
CMX	$0.6 < \eta < 1.0$	6.2	1.4 GeV/c
IMU	$1.0 < \eta < 1.5$	6.2-20	1.4-2.0 GeV/c

Table 3.4: Pseudorapidity coverage, pion interaction length, and minimum detectable p_T for the different muon sub-detectors of CDF II.

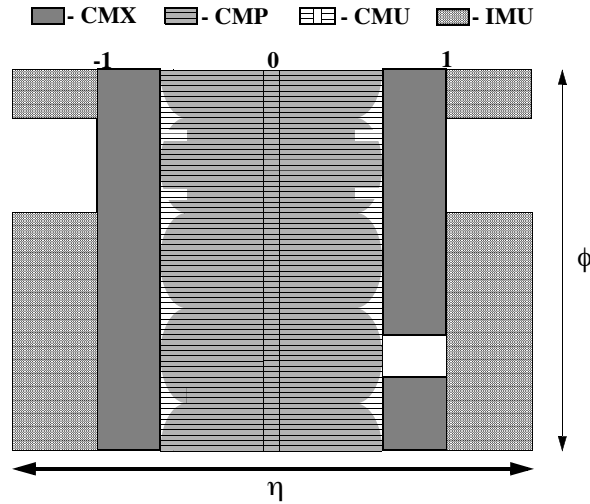


Figure 3.8: Coverage in η - ϕ of each muon system.

and protons by measuring the time it takes these particles to travel from the primary vertex of the $p\bar{p}$ collision to the TOF system. The main physics motivation for the introduction of this detector sub-system is to enhance particle identification for flavor tagging.

The TOF system consists of 216 scintillator bars, approximately 280 cm long and with a cross-section of 4 cm \times 4 cm. The bars are arranged into a barrel at a radius of about 138 cm, and in the 4.7 cm of radial space between the COT cylinder and the cryostat of the superconducting solenoid. The pseudorapidity coverage is roughly $|\eta| < 1$. The scintillator bars are read out at both ends by fine-mesh photomultiplier tubes (PMT; Hamamatsu R7761), which provide a gain of $\sim 30,000$ inside the 1.4 Tesla magnetic field of the CDF solenoid.

Particles passing through the scintillating material of the bars deposit energy causing small flashes of visible light detected by the PMT. The signal from the photomultiplier tube is processed by a pre-amplifier circuit mounted directly onto the tube, and sent to the readout electronics in the collision hall. The readout electronics perform both time and amplitude

digitization of the signal. The TDC information is a digitization of the time when the pulse leading edge reaches a fixed discriminator threshold. This time depends on the amplitude of the pulse, as larger pulse heights fire the discriminator at an earlier time than smaller pulse heights (*time-walk*). Larger pulses also give better timing resolution, as light attenuates while travelling through the scintillator material. Therefore, particles passing through the bar near the photomultiplier tube have better timing resolution than those which are farther away.

Particle identification

The TOF system expands CDF's particle identification (PID) capability. Along with the measurement of specific ionization dE/dx in the COT, the measurement of the particle's flight time provides complementary particle discrimination power in the low p_T region.

PID with TOF is performed by measuring the time of arrival t_{flight} of a particle at the scintillator with respect to the collision time, t_0 . The particle's mass m is then determined as

$$m = \frac{p}{c} \sqrt{\frac{c^2 t_{\text{flight}}^2}{L^2} - 1}, \quad (3.8)$$

where the track's momentum p and path length L between the beam collision point and the scintillator are measured in the tracking system.

The achieved timing resolution relies on the calibration of the response of each channel. The time t_i at which the discriminator of channel i is fired, for a track hitting the scintillator at a position z along the length of the bar, is described by

$$t_i = \alpha_i + t_0 + t_{\text{flight}} + \frac{1}{c_s} \left(\frac{l}{2} \pm z \right) - S_i(Q_i), \quad (3.9)$$

where the constant offset α_i accounts for cable and electronics delays, l is the length of the scintillator bar, c_s is the effective speed of light propagation in the scintillator, and the last term describes the effect of time-walk introduced by the use of leading edge pulse discriminators, which depends on the integrated charge Q_i of the PMT pulse. The positive (negative) sign multiplying the z hit coordinate corresponds to the case where a PMT is on the positive z (negative z) end of the bar.

The TOF resolution may be estimated from the difference between the time of flight measured for each track t_{flight} , and the expected time of flight assuming the track is a pion. The calculation is improved by computing the expected flight time assuming various particle hypotheses with specific probabilities (f_π , f_k and f_p for pions, kaons and protons, respectively). Additionally, the resolution for any given channel degrades with the hit displacement from the photomultiplier tube; a linear parameterization in z suitably accounts for the effect. The timing resolution at the face of the PMT is about 110 ps.

3.3 Data acquisition and trigger systems

The Tevatron proton and antiproton bunches cross every 396 ns at the center of the CDF detector. Such a high collision rate, of about 2.5 million interactions per second, makes it not practical to store information about every single $p\bar{p}$ collision. The readout of the entire detector produces an event size of the order of 200 kB, which would thus require a data recording rate of 0.5 GB/s and would amount to a few hundred tera-bytes of data in a single week of running. Furthermore, the time it takes to read the entire detector out, about 2 ms, would be long enough for another 5,000 or so interactions to take place. However, most processes of interest have cross sections at least three orders of magnitude smaller than the total $p\bar{p}$ cross section (at $\sqrt{s} = 1.96$ TeV). The total hadronic cross section (including elastic, inelastic, and diffractive processes) is about 75 mb, while for instance the $b\bar{b}$ production cross section is only about 0.1 mb. This makes it possible to circumvent the above mentioned difficulties by reading out and storing only events with signatures found of interest. The process of real-time event selection is referred to as *trigger*.

The data acquisition (DAQ) and trigger systems are intrinsically coupled providing a common infrastructure for data taking. The design of the pipelined DAQ system and three-level staged deadtimeless trigger is represented in Figure 3.10. An event is passed on to the following trigger level if it has been accepted by the previous stage, being otherwise discarded. The input event rate is reduced at each level, providing increasing time for more complex and accurate reconstruction tasks.

The first level of the trigger, Level 1, rejects the vast majority of the events. A period of 5.5 μs is allowed for Level 1 to reach its decision. The necessary delay is attained through pipeline storage of the readout data available at the front-end electronics. The buffers are 14 (396 ns) bunch crossings deep, and for every Tevatron clock cycle, the event is moved up one slot in the pipeline. By the time it reaches the end of the pipeline the trigger will have reached a decision whether to accept or reject the event. The Level 1 decision is based on only a subset of the detector parts along with quick pattern recognition and filtering algorithms. The original 2.5 MHz event rate is reduced at Level 1 to less than 50 KHz. Events accepted by Level 1 trigger are moved to one of four on-board Level 2 buffers. The second trigger level performs a limited event reconstruction through a more careful analysis of the readout information. It also takes longer, about 20 – 30 μs , to reach a decision. To ensure maximal speed, both Level 1 and Level 2 triggering mechanisms are implemented with custom designed electronics. The DAQ system allows the Level 2 trigger to accept as many as 300 events per second. Following a Level 2 accept, the various detector data fragments are assembled together by the Event Builder (EVB) system to be transferred to the last

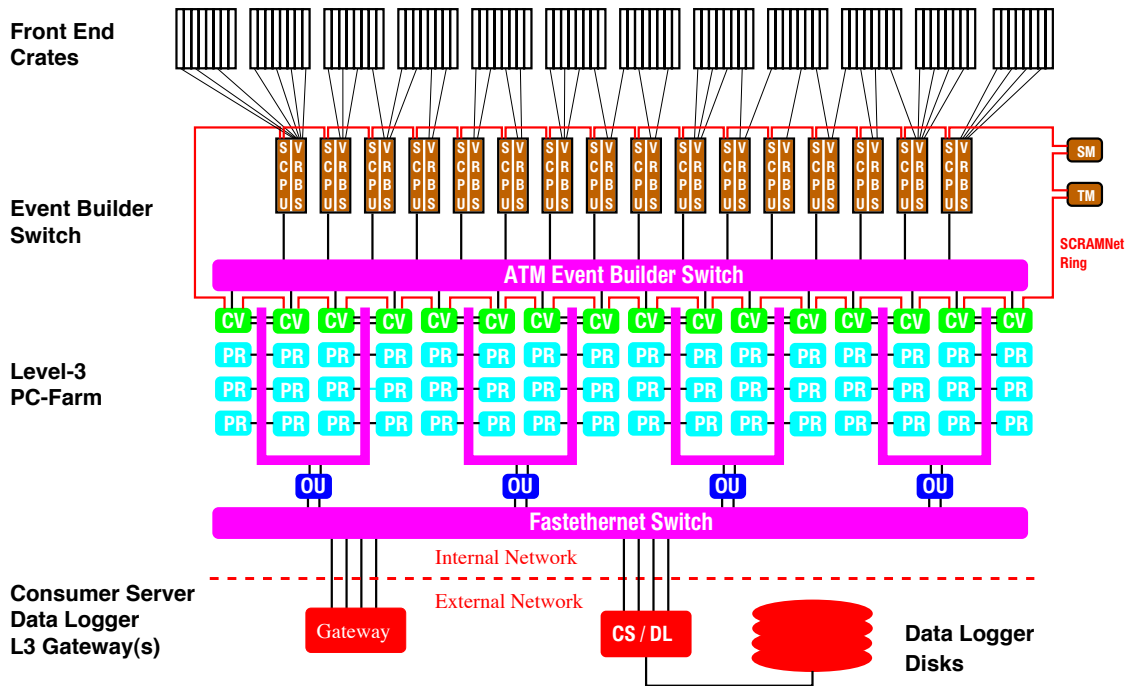


Figure 3.9: Representatio of the DAQ system layout: event building and Level 3 filtering.

trigger stage. The third level of the trigger, Level 3, is implemented as a PC computing farm. Parallel event processing by many nodes allows for nearly 1 s to be allocated for the trigger decision, permitting a fairly thorough event reconstruction. An event rate below 75 Hz is achieved at the end of the final trigger level.

A set of requirements that an event has to fulfill at Level 1, Level 2 and Level 3 constitutes a *trigger path*. The CDF trigger system implements about an hundred trigger paths, which compete for DAQ bandwidth. An event will be accepted if and only if it passes the requirements of any one of these paths. Events accepted by the trigger get written to a mass storage device.

All data manipulations performed from then on are referred to as data handling. These include offline reconstruction of physics objects, such as tracks, vertices, electrons, muons, jets, *etc.*, suitable for data analysis. This stage, denominated *production*, involves similar operations to those performed at Level 3, only with more elaborate algorithms, and using the most accurate and up-to-date detector calibrations and alignments.

3.3.1 Data flow

The DAQ system is responsible for collecting the data fragments from the front-end electronics systems, for events satisfying the trigger criteria, up to the final stage in which complete

event records are formed and sent to mass storage.

The front-end and trigger electronics are packaged as VME modules that reside in about 120 crates in the system. These modules process detector signals and make the data available to the DAQ system through the VME bus. Each front-end crate contains at least one processor board for hardware initialization and event readout, running under the VxWorks operating system. The crates contain also a *controller* module which distributes, through the VME backplane, received timing synchronization signals. These timing signals are dictated by the Tevatron clock, coherently with the bunch crossings, and ensure global synchronization of readout electronics and trigger.

The controller module further provides the interface of the VME modules to the Trigger System Interface (TSI), as well as the data interface to the EVB. The TSI is responsible for receiving the decisions from the hardware triggers (Level 1 and Level 2), communicating them to the front-end crates, and supervising the data flow up until it is transferred to the EVB.

Event building and processing farm

Upon Level 2 accept, the data from the various front-end crates are collected and transmitted to the Level 3 trigger by the event builder system. The EVB and the Level 3 form a crucial and intricate system of fast data transmission and control networks, and processing units, whose structure is outlined in Figure 3.9.

The data are first received by the VME Readout Boards (VRB). Each VBR is fiber linked to a group of front-end crates. The VRB are themselves part of 15 EVB crates, each of which is controlled by a single board processing unit referred to as “Scanner CPU” (SCPU) running VxWorks. The 15 EVB crates are connected to 16 *converter* node PCs of the Level 3 farm through an Asynchronous Transfer Mode (ATM) network switch for data transfer. Data flow between the SCPUs and converter nodes is controlled by the Scanner Manager (SM). The SM is a task running in a processing unit located at an additional EVB crate, and constitutes the EVB interface with the TSI. Communication among the SCPUs, converter nodes and TSI is performed over a serial-ring reflective-memory control network denominated SCRAMNet (“shared common random access memory network”).

Event building and data transfer from the front-end electronics to the Level 3 involve the following stages. Front-end processors complete data readout and, via the controller module, load data to the VRBs. The TSI passes the Level 2 accept message to the SM. The SM instructs the SCPUs to read in and combine the event fragments from all VRBs in their local crates. SCPUs acknowledge loading completion to the SM. Meanwhile, converter nodes if ready make their status known to the SM. The SM selects a single converter node among

Level 1

The Level 1 trigger is a synchronous system, providing an accept / reject decision every bunch crossing, using a fully pipelined architecture. The Level 1 decision is based on a limited amount of event information from the COT, calorimeters and muon chambers, which is used to form coarse versions of physics objects (such as tracks, electrons and muons) referred to as trigger *primitives*.

Track primitives are identified by the Extremely Fast Tracker (XFT) [48]. A rough measurement of the transverse momentum and azimuthal direction of a track is formed by using the hit information of the 4 axial superlayers of the COT. The identification process involves three stages: hit classification, segment finding and segment linking. Each wire hit is classified as either “prompt”, if the drift time is lower than 66 ns, or as “delayed”, if the drift time ranges from 66 ns to 220 ns. Track segments are searched for in each axial superlayer by grouping together adjacent COT cells in groups of 4 and by comparing the hit data to a list of pre-loaded patterns. The patterns vary depending on the combination of prompt and delayed hits and the track angle through the cell or track p_T . Each found segment is characterized by its mean ϕ position and slope information. Once track segments have been found, sets of four, each belonging to a different superlayer, are compared against a list of templates in a $\Delta\phi$ window of 1.25° . Matches are searched for which correspond to valid tracks with $p_T \geq 1.5$ GeV/c and constrained to the beamline. If no track is found, the search is performed on segments in the innermost three axial superlayers.

Finally, the XFT reports the tracks p_T , ϕ_6 (ϕ at the superlayer 6) and charge. The achieved XFT track resolution is $\sigma(p_T) = 1.7\%/GeV/c$ and $\sigma_{\phi_0} = 5$ mrad, only about a factor of 10 coarser than the offline reconstruction. If more than 6 tracks are found an automatic Level 1 accept is generated; otherwise the decision is dependent on the specific trigger requirements on p_T and ϕ accordingly coded in look-up tables.

The XFT tracks are extrapolated to the calorimeter and muon detector systems via the Extrapolator unit (XRTP) for matching with electron towers and muon stubs. The calorimeter trigger is based both on object primitives (electrons, photons and jets) and global event variables (total transverse energy $\sum E_T$ and missing transverse energy \cancel{E}_T). Primitives are formed by applying thresholds to individual calorimeter trigger towers. Transverse energy (E_T) is found by summing the digitized calorimeter data into trigger towers weighted by $\sin\theta$. Muon and dimuon primitives are derived from hits in the muon chambers or coincidences of hits with the scintillators. Track matching is performed at a granularity of about 1.5° .

Level 2

The Level 2 trigger is an asynchronous system which processes events accepted by Level 1 based on better precision and additional event information. Level 2 is implemented in two stages, with a latency of about $10 - 20 \mu s$ each, respectively achieved by primitive building hardware and by programmable processors (Alpha) which operate on the primitive inputs to perform further event topology characterization and impose tighter requirements.

The Silicon Vertex Trigger (SVT) [49] processor uses the $r-\phi$ hits in the silicon detectors to extend the XFT track primitives inside the SVX volume. It provides a measurement of the track impact parameter d_0 , while also improving the determination of p_T and ϕ_0 . It thus enables the trigger to distinguish primary and secondary particles, and hence to collect, in particular, large samples rich in heavy flavor decays.

The SVT structure reflects the SVX detector's 12-fold azimuthal symmetry and 3 barrel segmentation, and does tracking separately for each ϕ sector and barrel. An SVT track candidate requires coincidence of an XFT track and hits in four (out of the five available) silicon layers. The XFT tracks are swum into the SVX detector region, forming "roads" within which clusters of charge in the silicon layers have to be found. The SVT uses a list of pre-loaded patterns for finding the best coincidences. The information about the XFT outer-track and the four silicon hits is finally fed into a linearized fitter which returns the measurements of p_T , ϕ_0 and d_0 for the track.

The average SVT processing time is about $19 \mu s$ as indicated in Figure 3.11. The SVT impact parameter resolution for tracks with $p_T > 2 \text{ GeV}/c$ is about $35 \mu m$, comparable to that of offline tracks which do not use Layer 00 information (which is not yet available in the SVT). This is shown in Figure 3.11; the width of the Gaussian fit shown for the tracks impact parameter distribution is $47 \mu m$, which is the combination of the intrinsic SVT impact parameter resolution and the transverse size of the beam profile (about $30 \mu m$).

The calorimeter trigger is also improved at Level 2. Clustering of trigger towers is performed by applying seed and shoulder thresholds, which is used to form jets and reduce corresponding rates. The shower maximum strip chambers (CES) are further used to refine the track matching, and reduce the fake electron and photon rates.

Level 3

At Level 3 nearly offline quality of event reconstruction is achieved, taking advantage of the complete event record and improved resolutions not available to the lower levels. Tight matching of tracks to calorimeter and muon system information is implemented. Three dimensional track reconstruction becomes available for the first time. Vertices may be explicitly

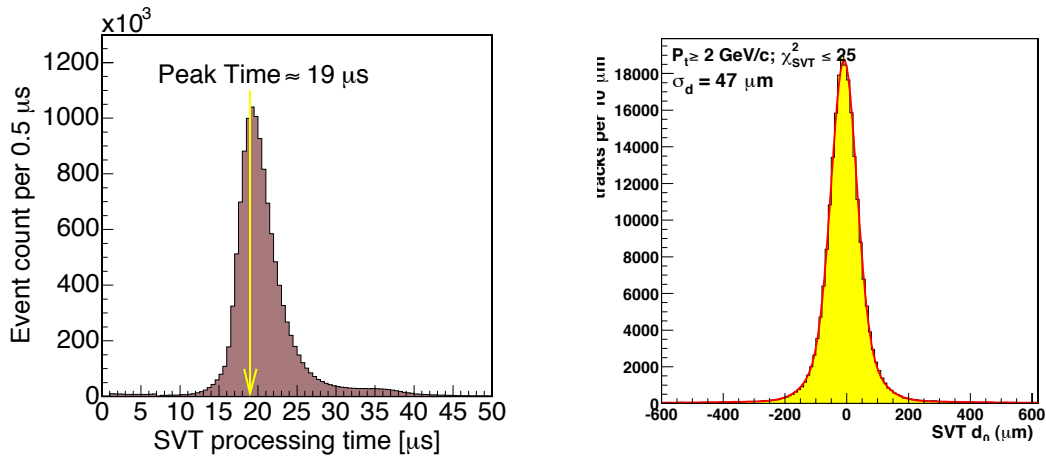


Figure 3.11: SVT processing time (left) and track impact parameter resolution (right).

reconstructed and L_{xy} extracted. Invariant masses of associated particle candidates, for instance, may also be used as trigger criteria. Results from the previous levels are used to drive the algorithms.

3.4 Résumé

The particle accelerator and detector systems, the Tevatron and CDF, are described. Their performance dictates the quantity, quality, and physics content of the data samples. The exquisite precision offered by the detector components is determining for the reach of the analysis. So too is the trigger system, responsible for selecting, in real-time, the events of interest from the remaining, much more abundant collision products. The prominent experimental signature explored is the displaced nature of the B meson decays, relative to the nominal position of the primary proton–anti-proton collision.